Supporting Information

Duan et al. 10.1073/pnas.1111297109

SI Results and Discussion

Specificity and Selectivity of the Copper Ion Enhancement Effect. Cyclization of **5** to **8**, with removal of two hydrogens, results in modest loss of activity (shape change). Significantly, further removal of four hydrogens from **8** giving 2-thiophenethiol (**9**), results in almost complete loss of odorant receptor (OR) activity, likely owing to the very poorly nucleophilic character of the thiophene exocyclic lone pair (1). Conversion of **1** to sulfone **10** also results in a partial loss of OR activity, owing to the inability of the sulfone group to coordinate to copper, even though the acidity of the thiol group is increased. On the other hand, most activity is retained when the thioether sulfur is replaced by selenium in **7** and on removal of two hydrogens giving dithioester **3**; good activity also remains with trithiocarbonate **12**. Thiol-thioether **13** shows even higher OR activity than (methylthio)methanethiol ($MeSCH_2SH$; MTMT) **1**, although the structure of its copper chelate would most likely be different from that of **1**. Thiol-thioether **4** is also active, although it also shows cell toxicity effects at higher concentrations. On the other hand, loss of OR activity is seen on methylation (**11**) of the thiol group of **1**, loss of the thioether methyl group (**18**), or isomerization to disulfide **14** or bisthiol **15**.

Copper Ions Are Not Required for the Biosynthesis of Functional MOR244-3. We investigated the temporal requirements of copper to enhance receptor activation, that is, whether adding copper ion during plasmid transfection or odorant stimulation makes a difference in the enhancement of receptor response. We found that when the cells were incubated with Cu^{2+} starting at transfection and then washed to remove free Cu^{2+} before MTMT addition, the enhancement effect was lost compared with adding Cu^{2+} at the same time as MTMT during stimulation (Fig. S6*A*), indicating that copper ion was probably not bound to the receptor before MTMT addition. Similarly, if copper is incorporated into the receptor during OR protein synthesis, trafficking, or membrane insertion, depleting copper starting at transfection would negatively affect receptor activation, whereas eliminating copper only at stimulation would not. We therefore asked whether tetraethylenepentamine (TEPA) treatment beginning at transfection would affect receptor activation. We found that such chronic depletion of copper had no effect on activation, indicating that it is also unlikely that copper is incorporated into the OR as a part of its biosynthesis (Fig. S6*B*). Furthermore, the evidence from the real-time GloSensor experiments also supported the notion that copper acts acutely along with MTMT to stimulate the receptor (Fig. 2*C*).

We then investigated the feasibility of an intracellular origin of copper, for example, as regulated by the copper-transporting ATPases ATP7A and ATP7B that aid in the secretion of cuproenzymes by loading copper in the *trans*-Golgi network (6). To delineate the possibility of copper-loading from inside the cell, we used a knockdown cell line stably expressing RNAi constructs of ATP7A and ATP7B in HEK293T cells (Fig. S6 *C* and *D*). The most effective clone knocked down almost 100% of ATP7A and at least 50% of ATP7B. By comparing the dose–response curve of MOR244-3 transfected into the knockdown cell line with wild-type HEK293T cell line, we found that knocking down the intracellular copper efflux transporters ATP7A and ATP7B did not affect the copper ion enhancement effect on the response of MOR244-3 to MTMT (Fig. S6*D*). Although we cannot exclude the possibility that residual ATP7B might be sufficient for the copper-loading of the OR, the data are consistent with the idea that copper is not required for the biosynthesis of functional MOR244-3.

Additional Discussion of Copper Complexes. Fig. S7 and Table S5 provide information on representative copper thiolates. In addition, X-ray structures have been reported for copper complexes of other compounds related to MTMT and its analogs. Notably, Black et al. (2) identified a crystallized complex between copper ion and bis-(methylthio)methane (**11**), which elicited a weak response with copper effect by MOR244-3 in our system. The copper–bis(methylthio)methane complex contained two copper ions coordinated by two dithioether molecules, forming an octagonal ring in a chair conformation. Similar tetrameric copper–thiol complexes have been previously proposed with sterically hindered thiols (Table S5, entry 18). Among the other MOR244-3 ligands, 2-mercaptomethylpyridine forms complexes with zinc (3), and cysteamine forms a dimeric complex with copper (4). Copper complexes of MOR244-3 ligands methyl dithioformate (**3**) and dimethyl trithiocarbonate (**12**) may share similarities with copper complexes of carbon disulfide (5).

SI Materials and Methods

Additional Chemicals. MTMT and its analogs, including (ethylthio)-methanethiol (**2**), 2-(methylthio)ethanethiol (**17**), 1-(ethylthio)-ethanethiol (**5**), thiolane-2-thiol (**8**), 1-(methylsulfonyl)methanethiol (**10**), and 3-(methylthio)-1-propanethiol (**13**), were synthesized according to previous reports (7–12). See below for the syntheses of [(1,1,-dimethylethyl)thio]methanethiol (**6**) and (methylseleno)methanethiol (**7**).

Clones and Mutagenesis. Our mouse OR library comprises 219 mouse ORs that represent more than 21% of the total 1,035 mouse OR genes and includes at least one member of most of the 228 mouse OR subfamilies as previously defined (13). The ORs, along with an N-terminal rhodopsin tag, were cloned into the pCI mammalian expression vector, as described previously (14). MOR244-3 site-directed mutagenesis was carried out using overlap extension PCR. The identities of all constructs were confirmed by sequencing.

Patch Clamp. Genetically targeted SR1-IRES-tauGFP mice, kindly provided by Dr. Peter Mombaerts (Max Planck Institute of Biophysics, Frankfurt, Germany) (15), were used for patch clamp recordings from the septal organ neurons. This strain is in a mixed 129 and C57BL/6 genetic background, and 3- to 5-wk-old mice of either sex were used. All procedures were approved by the Institutional Animal Care and Use Committee at the University of Pennsylvania.

Intact epithelial preparations were prepared as in our published procedures (16, 17). Mice were deeply anesthetized by i.p. injection of ketamine (200 mg/kg) and then decapitated. The head was immediately put into ice-cold Ringer's solution, which contained (in mM): NaCl 124, KCl 3, $MgSO_4$ 1.3, $CaCl_2$ 2, $NaHCO_3$ 26, NaH_2PO_4 1.25, glucose 15; pH 7.6 and 305 mOsm. The pH was kept at 7.4 after bubbling with 95% O_2 and 5% CO_2. The nose was dissected out *en bloc*, and the olfactory mucosa attached to the nasal septum and the dorsal recess was removed and kept in oxygenated Ringer. Before use, the entire mucosa was peeled away from the underlying bone and transferred to a recording chamber with the mucus layer facing up. While recording, oxygenated Ringer was continuously perfused at 25 ± 2 °C.

The dendritic knobs of olfactory sensory neurons (OSNs) were visualized through an upright microscope (Olympus BX51WI) with a 40× water-immersion objective. An extra 4× magnification was achieved by an accessory lens in the light path. The GFP-tagged cells were visualized under fluorescent illumination. Superimposition of the fluorescent and bright-field images allowed

identification of nonfluorescent (non-SR1) cells under bright field, which directed the recording pipettes.

Electrophysiological recordings were controlled by an EPC-10 amplifier combined with Pulse software (HEKA Electronic). Perforated patch clamp was performed on the dendritic knobs by including 260 μM nystatin in the recording pipette, which was filled with the following solution (in mM): KCl 70, KOH 53, methanesulfonic acid 30, EGTA 5.0, Hepes 10, sucrose 70; pH 7.2 (KOH) and 310 mOsm. The junction potential of −9 mV was corrected in all experiments offline. Under voltage-clamp mode, the signals were initially filtered at 10 kHz and then at 2.9 kHz. For odorant-induced transduction currents under voltage-clamp mode, the signals were initially filtered at 2.9 kHz and sampled at 333 Hz. Further filtering at 60 Hz did not change the response kinetics or amplitudes, indicating that the sampling rate was sufficient and that signal aliasing was not a concern. A seven-barrel pipette was used to deliver stimuli by pressure ejection through a picospritzer (Pressure System IIe, Toohey Company). All compounds were diluted in Ringer's solution.

Olfactory Discrimination Test. Olfactory discrimination test was performed with modifications to previously published protocols (18, 19). All procedures were approved by the Institutional Animal Care and Use Committee at Shanghai Jiaotong University School of Medicine. Sixteen experimentally naïve, 8-wk-old, male adult C57BL/6J mice were maintained on a reverse light/dark schedule. Four days before training and during training and testing, the mice were weighed and fed daily to maintain ≈80–85% of their free-feeding weight. The mice are trained by receiving four to six 10-min trials for 6 d to associate either eugenol or MTMT with sugar reward; half of the trials were with an odorant paired with sugar and half with the other odorant without sugar. The order of odor presentation was randomized across days. During the training, the odorant was presented on a piece of filter paper (25 mm in diameter; Whatman) placed on the bottom of a sealed 60-mm Petri dish with holes drilled on the top, which is placed in the center of the training cage and buried in wood chip bedding. During the trials paired with sugar reward, three to six small sugar pieces were scattered on the top of the Petri dish. On the day of testing, TEPA or dH_2O was gently applied to both nostrils of mice under ketamine (90 mg/kg) and xylazine (10 mg/kg) anesthesia using a modified pipette tip. After recovery from anesthesia, each mouse was allowed to be habituated to the testing cage (1,380 × 670 × 1,950 mm) for 2 min before testing. During testing, the odorants were presented on filter paper, placed in closed biopsy cases without sugar, and buried at a depth of 3 cm in wood chip bedding on opposite ends of the testing cage. A fresh testing cage and bedding were used for each test trial. Mouse behavior was recorded in the dark with a digital video camera with infrared illumination. Investigation was defined as the animal pointing its nose directly at the odorant container and digging with front paws. Paired *t* test was used to look for differences in investigation time.

(Methylseleno)methanethiol (7). Selenium powder (2.4 g, 30 mmol), dry tetrahydrofuran (35 mL), and methyllithium (1.4 M in diethyl ether; 30 mmol) in a 250-mL three-necked flask were stirred at room temperature for 10 min under argon, cooled to −78 °C, and treated with chloroiodomethane (31.5 mmol). The solution was warmed to room temperature and stirred for a total of 2.5 h. Analysis by GC-MS indicated the presence of a major component with *m/z* 143 (six Se isotopes associated with this M^+). Without further purification, potassium thioacetate (37.5 mmol) was added, and the mixture was stirred at room temperature for 24 h to give, after concentration, extraction with methylene chloride, and concentration, 2.32 g (42% yield) of ethanethioic acid, *S*-[(methylseleno)methyl] ester as a liquid. The crude product, purified by column chromatography (hexane/ethyl acetate 95:5), showed GC-MS (electron impact) *m/z* 184 (M^+); ^{1}H NMR (300 MHz) δ 2.06 (s, 3H), 2.33 (s, 3H), 3.90 (s, 2 H); ^{13}C NMR (75.3 MHz) δ 5.21 (d, J = 20 Hz), 20.51, 30.19, 194.97.

A 890 mg (4.88 mmol) portion of ethanethioic acid, *S*-[(methylseleno)methyl] ester was dissolved in 50 mL of anhydrous ether, cooled under argon to −78 °C, and treated with lithium aluminum hydride (93 mg, 2.4 mmol). The reaction mixture was stirred for 30 min, warmed to room temperature, and cautiously treated with 10% aqueous HCl, extracted with ether (2 × 30 mL), and the separated ether extract was dried ($MgSO_4$) and concentrated to give the title compound, a liquid with a strong, pungent odor (640 mg, 93% yield), ^{1}H NMR (300 MHz) δ 2.00 (t, J = 8 Hz, 1H), 2.14 (*d*, J = 1.9 Hz, 3H), 3.60 (dd, J = 1.3; 7.9; 2H); ^{13}C NMR (75.3 MHz) δ 4.99, (d, J = 21 Hz), 16.87; IR (KBr) 2921 (s), 2532 (m, S–H), 1419, 1182, 908, 732 cm^{-1} (all s); GC-MS (electron-ionization mode) 142 (M^+, 40%), 109 (20%), 93 (25%), 47 (100%). By comparison (methylthio)-methanethiol (**1**) shows IR (KBr) 2913 (s), 2544 (m, S–H), 1435, 1422, 1215, 987, 745, 698 cm^{-1} (all s); ^{1}H NMR (300 MHz) δ 1.86 (t, J = 8 Hz, 1H), 2.22 (s, 3H), 3.64 (d, J = 8.0 Hz; 2H).

[(1,1,-Dimethylethyl)thio]methanethiol (6). *N*-Chlorosuccinimide (13.8 g, 0.103 mol) was added in portions to an ice-cold solution of commercial *tert*-butyl methyl sulfide (10 g, 0.096 mol) in CCl_4 (240 mL), and the reaction was stirred at the same temperature for 1 h while being monitored by NMR. The solution was brought to room temperature and stirred for an additional 2 h. The CCl_4 was distilled off first at atmospheric pressure and then under vacuum giving *tert*-butyl chloromethyl sulfide as a colorless liquid (6.2 g), which was used without further purification in the next step. The chloride (1.1 g, 0.0079 mol) was refluxed with thiourea (1.2 g, 0.015 mol) in EtOH (10 mL) for 48 h. The solvent was evaporated, and the residue was redissolved in water (10 mL). The solution was stirred with 40% NaOH (8 g in 20 mL) for 15 min at room temperature followed by acidification with 2N HCl and extraction with diethyl ether (3 × 30 mL). The organic layers were combined and dried (Na_2SO_4), and the solvent was removed by distillation. Vacuum distillation afforded pure thiol as a colorless liquid with an unpleasant odor (1.2 g; 59%). The title compound showed ^{1}H NMR ($CDCl_3$) δ 1.27 (s, 9H), 1.98 (m, 1H), 3.67 (d, J = 10.4 Hz, 2H); ^{13}C NMR δ 23.9, 30.8, 44.1; GCMS *m/z* 136 (M^+).

Flow Cytometry Analysis. Flow cytometry analysis for the cell-surface expression of MOR244-3 and its mutants in Hana3A cells was performed as previously described (20).

Measurement of Copper Concentrations in Mouse Mucus and the Stimulation Medium. Nasal mucus collection was performed as previously described (18). Briefly, Ringer's solution [≈50 μL, containing the following (in mM): 140 NaCl, 5.6 KCl, 10.0 Hepes, 2.0 pyruvic acid sodium salt, 1.25 KH_2PO_4, 2.0 $MgCl_2$, 2.0 $CaCl_2$, 9.4 glucose] was injected into the dorsal area of the nasal cavity of adult BALB/C mice under ketamine (90 mg/kg) and xylazine (10 mg/kg) anesthesia using a modified pipette tip. The nasal lavage fluid was immediately collected using the same tip by pipetting in and out. The mucus fluid and CD293 stimulation medium were treated with a concentrated acid mixture overnight and then subjected to inductively coupled argon plasma-mass spectroscopy.

Homology Modeling. The X-ray crystal structure of the turkey β1 adrenergic receptor (Protein Data Bank entry 2VT4, resolution 2.7 Å) (21) was used as the template to construct the human MOR244-3 protein. The sequence of the human MOR244-3 was retrieved from UniProt (http://www.uniprot.org/uniprot/Q9R0K3). According to the secondary structure information of the template, the sequence alignment was adjusted manually to obtain a more reasonable alignment. A 3D model of the human MOR244-3 protein was generated using Modeler (version 9v2) (22).

1. Koczaja-Dailey KM, Luo S, Rauchfuss TB (1996) Acid-base chemistry of transition-metal-π-thiophene complexes. *Transition Metal Sulfur Chemistry,* ACS Symposium Series, eds Stiefel EI, Matsumoto K (American Chemical Society, Washington, DC), Vol 653, Ch 9, pp 176–186.
2. Black JR, Champness NR, Levason W, Reid G (1996) Self-assembly of ribbons and frameworks containing large channels based upon methylene-bridged dithio-, diseleno-, and ditelluroethers. *Inorg Chem* 35:4432–4438.
3. Burth R, Vahrenkamp H (1998) Zinc thiolate complexes with chelating nitrogen ligands. *Inorg Chim Acta* 282:193–199.
4. Loeb B, Crivelli I, Andrade C (1995) A violet mixed-valence copper mercaptoethylamine complex generated electrochemically or by reversible interaction with oxygen. *Inorg Chim Acta* 231:21–27.
5. Haack P, Limberg C, Tietz T, Metzinger R (2011) Unprecedented binding and activation of CS_2 in a dinuclear copper(I) complex. *Chem Commun (Camb)* 47:6374–6376.
6. Linz R, Lutsenko S (2007) Copper-transporting ATPases ATP7A and ATP7B: Cousins, not twins. *J Bioenerg Biomembr* 39:403–407.
7. Newman BC, Eliel EL (1970) Reduction with metal-ammonia combinations. III. Synthesis of β- and γ-alkylthiomercaptans from 1,3-dithiolanes and 1,3-dithianes. *J Org Chem* 35:3641–3646.
8. Anklam E, Aced A (1990) NMR and mass spectroscopic studies on normal-(alkylthio)-1-alkanethiols. *J Agric Food Chem* 38:123–125.
9. Matsumoto K, Costner EA, Nishimura I, Ueda M, Willson CG (2008) High index resist for 193 nm immersion lithography. *Macromolecules* 41:5674–5680.
10. Schutte L (1971) One-step synthesis of dithiohemiacetals a new class of compounds. *Tetrahedron Lett* 12:2321–2322.
11. Gais HJ (1977) Cyclic dithiohemiacetals—synthesis and properties. *Angew Chem Int Ed* 16:196–197.
12. Block E, Aslam M (1985) Serendipitous synthesis of alkyl trimethylsilyldithioformates by trapping of bis(trimethylsilyl)thione with alkanesulfenic acids. Synthesis of bis- and tris(trimethylsilyl)methanethiols. *Tetrahedron Lett* 26:2259–2262.
13. Zhang X, Firestein S (2002) The olfactory receptor gene superfamily of the mouse. *Nat Neurosci* 5:124–133.
14. Saito H, Kubota M, Roberts RW, Chi Q, Matsunami H (2004) RTP family members induce functional expression of mammalian odorant receptors. *Cell* 119:679–691.
15. Grosmaitre X, et al. (2009) SR1, a mouse odorant receptor with an unusually broad response profile. *J Neurosci* 29:14545–14552.
16. Grosmaitre X, Vassalli A, Mombaerts P, Shepherd GM, Ma M (2006) Odorant responses of olfactory sensory neurons expressing the odorant receptor MOR23: A patch clamp analysis in gene-targeted mice. *Proc Natl Acad Sci USA* 103:1970–1975.
17. Ma M, Chen WR, Shepherd GM (1999) Electrophysiological characterization of rat and mouse olfactory receptor neurons from an intact epithelial preparation. *J Neurosci Methods* 92:31–40.
18. Nagashima A, Touhara K (2010) Enzymatic conversion of odorants in nasal mucus affects olfactory glomerular activation patterns and odor perception. *J Neurosci* 30: 16391–16398.
19. Schellinck HM, Forestell CA, LoLordo VM (2001) A simple and reliable test of olfactory learning and memory in mice. *Chem Senses* 26:663–672.
20. Zhuang H, Matsunami H (2007) Synergism of accessory factors in functional expression of mammalian odorant receptors. *J Biol Chem* 282:15284–15293.
21. Warne T, et al. (2008) Structure of a β_1-adrenergic G-protein-coupled receptor. *Nature* 454:486–491.
22. Martí-Renom MA, et al. (2000) Comparative protein structure modeling of genes and genomes. *Annu Rev Biophys Biomol Struct* 29:291–325.

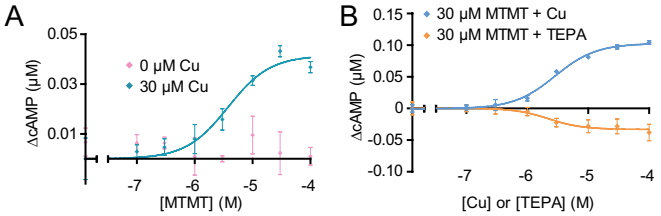

Fig. S1. Direct measurement of the change in cAMP level after MOR244-3 activation. (*A*) MOR244-3 was stimulated with increasing concentrations of MTMT with or without 30 μM copper ion. (*B*) MOR244-3 was stimulated with 30 μM MTMT with increasing concentrations of copper ion or TEPA. The *y* axis represents change in cAMP, shown as mean ± SEM (n = 6).

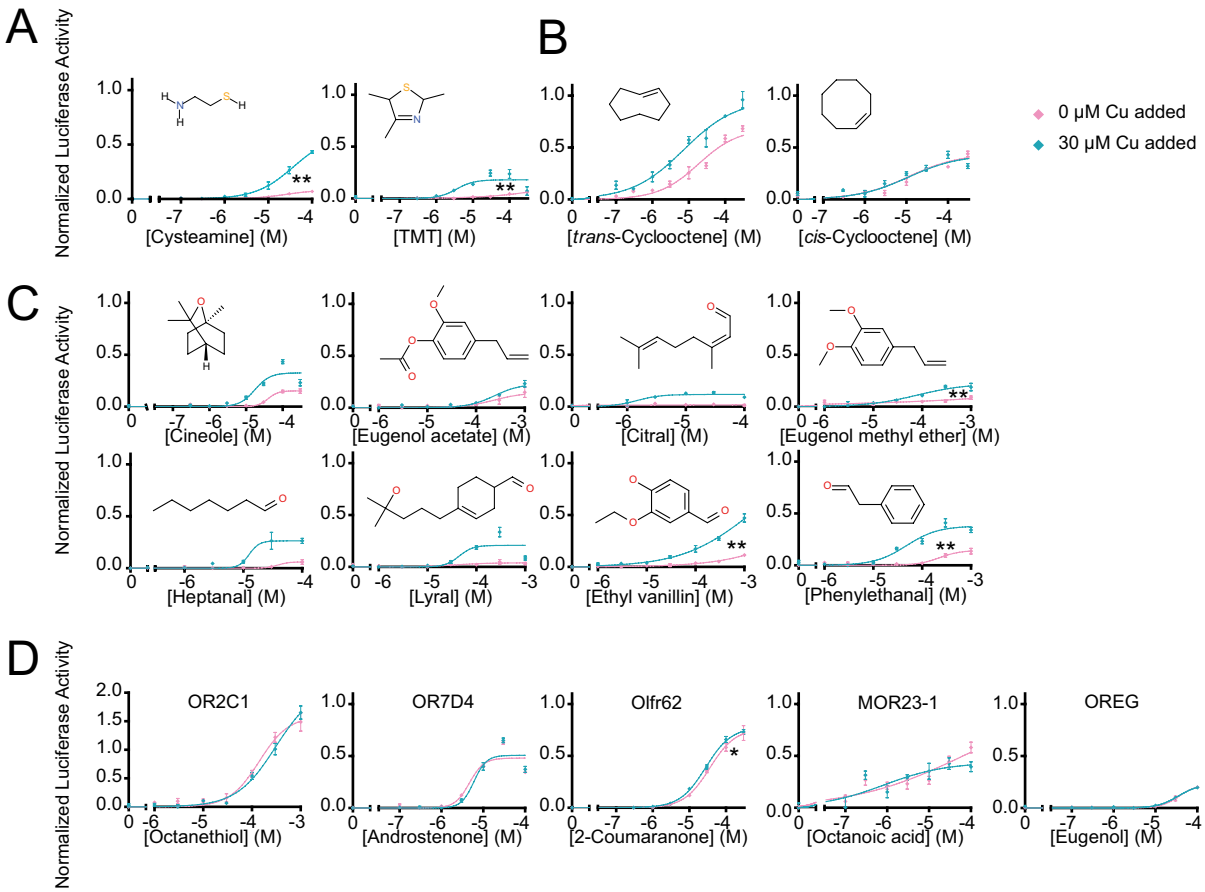

Fig. S2. Enhancement of OR activation by copper ion is specific to MOR244-3. Dose–response curves of MOR244-3 to (*A*) additional sulfur-containing compounds, (*B*) the strained olefin, *trans*-cyclooctene, and its unstrained isomer *cis*-cyclooctene, (*C*) other nonsulfur compounds, and (*D*) of other known receptor–ligand pairs with or without exogenous copper ion. The chemical structures of the respective compounds used for MOR244-3 are shown in the upper left-hand corners. All responses are normalized to MOR244-3's highest response to MTMT. *F* tests were used to compare the best-fit values of EC_{50}, top, and Hill slope between the pairs of dose–response curves with or without copper. Asterisks represent significance of *P* values after Bonferonni corrections. $*P < 0.05$, $**P < 0.01$ ($n = 3$).

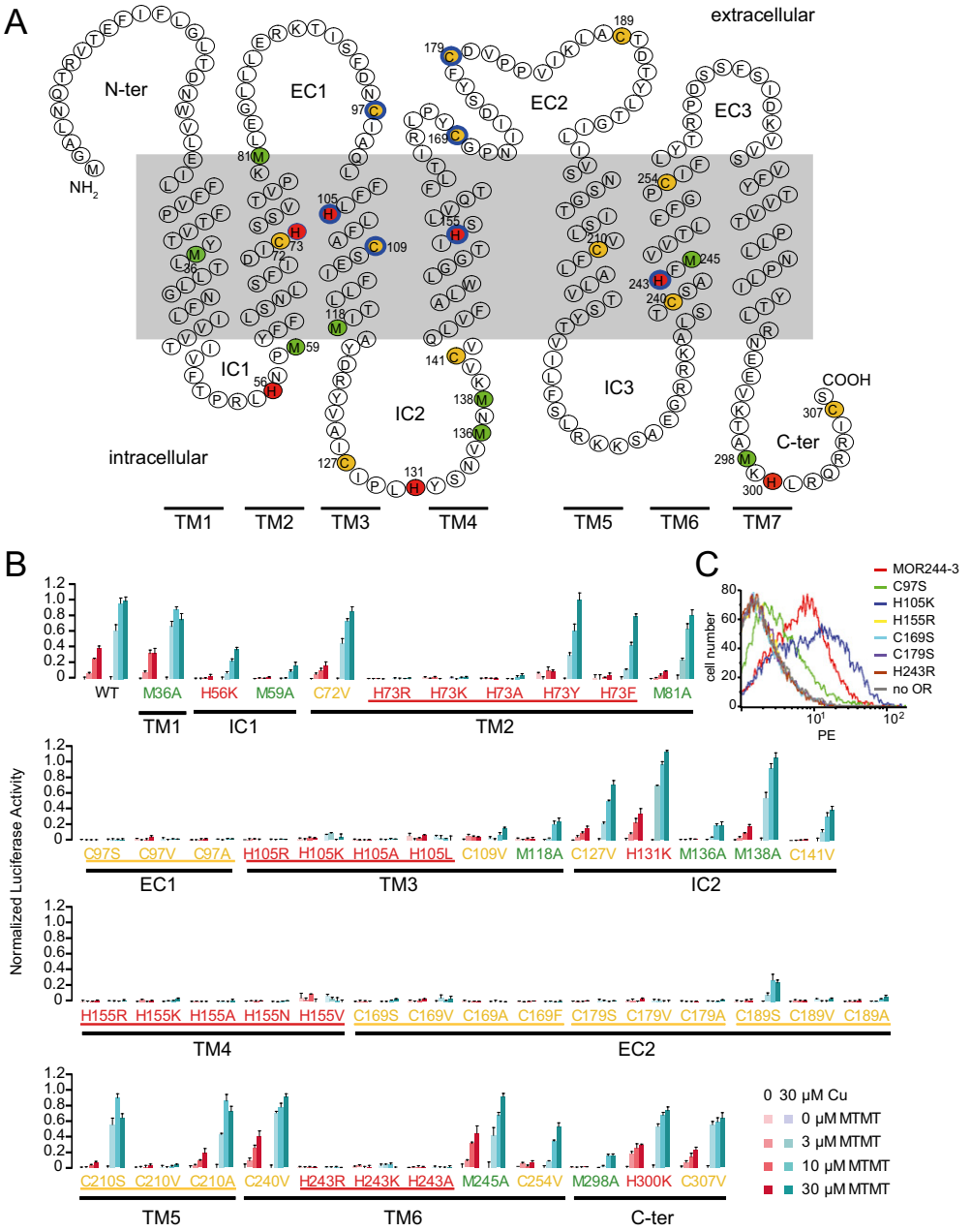

Fig. S3. Candidate copper-binding sites in MOR244-3 in response to MTMT as defined in a mutagenesis analysis. (*A*) A serpentine model of the MOR244-3 receptor color-coded for the methionine (green), histidine (red), and cysteine (yellow) residues that were subjected to the mutagenesis analysis. Residues circled in blue are those that exhibited complete loss-of-function phenotypes in the luciferase assay in *B*. Transmembrane domains are indicated by "TM". (*B*) Responses of all candidate copper-binding site mutants to three concentrations of MTMT with or without copper ion addition. Underscores indicate different mutations on the same residues. All responses are normalized to the wild-type MOR244-3's highest response to MTMT. (*C*) Flow cytometry analysis of the cell-surface expression of six of the complete loss-of-function mutants in Hana3A cells. The intensity of PE signal among the GFP-positive population was measured and plotted.

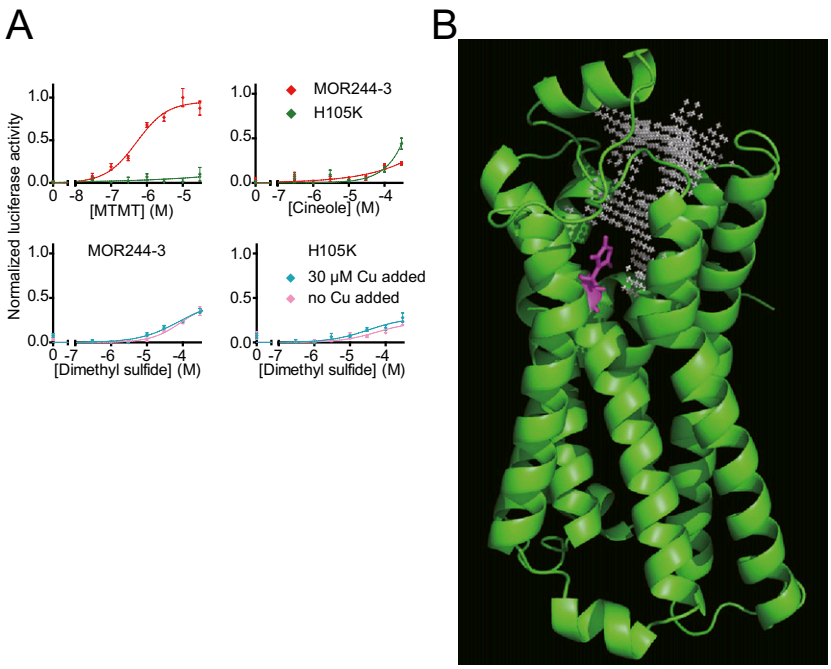

Fig. S4. Histidine 105 may be a copper-binding residue in MOR244-3. (*A*) *Upper*: Responses of the wild-type MOR244-3 and the H105K mutant to MTMT and cineole with 30 μM of exogenous copper. *Lower*: Response of wild-type MOR244-3 and the H105K mutant to dimethyl sulfide with and without 30 μM of exogenous copper. (*B*) Homology model of MOR244-3 with the predicted binding pocket depicted in white and the H105 residue in fuchsia.

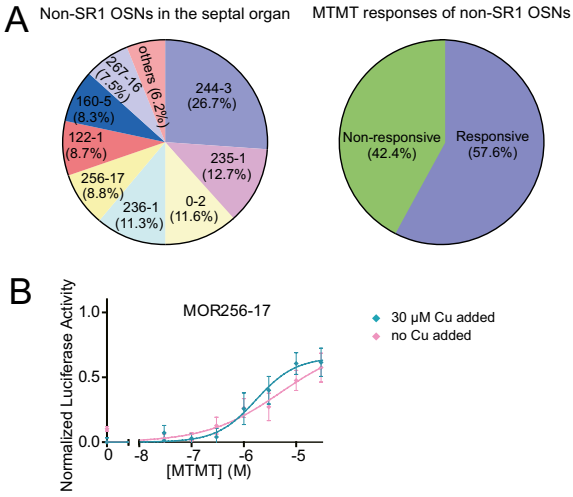

Fig. S5. MTMT-responsive ORs among the non-SR1 cells in the septal organ (SO). (*A*) *Left*: Composition of non-SR1 cells in the SO quantified from in situ hybridization data [modified from Tian and Ma (1)]. *Right*: MTMT-responsive cells in the SO. (*B*) Dose–response curves of a septal organ OR, MOR256-17, to MTMT with or without exogenous copper ion.

1. Tian H, Ma M (2008) Differential development of odorant receptor expression patterns in the olfactory epithelium: A quantitative analysis in the mouse septal organ. *Dev Neurobiol* 68: 476–486.

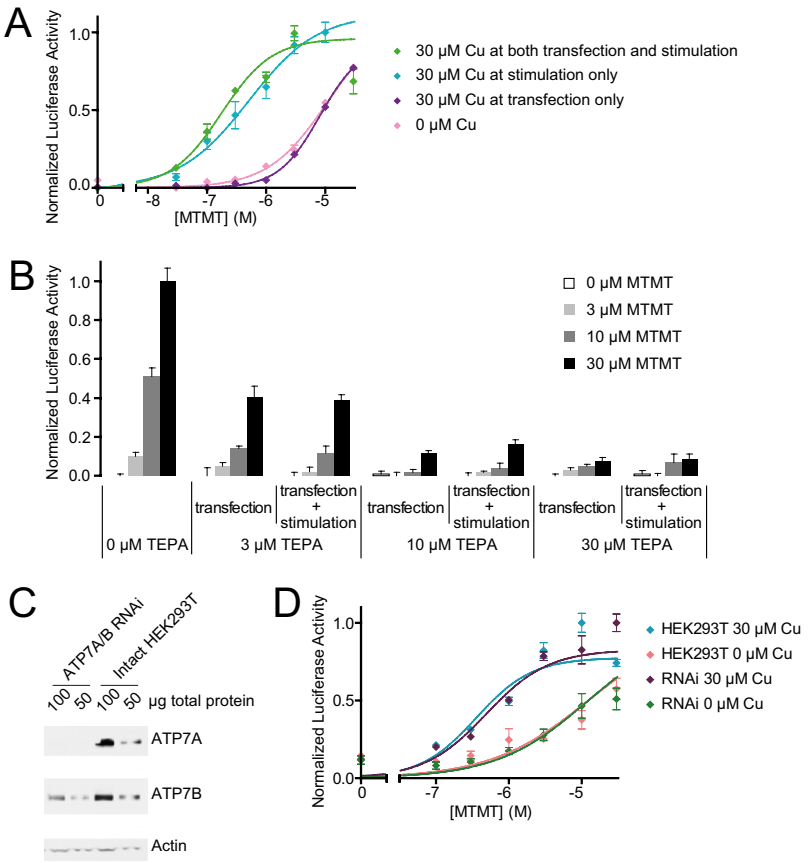

Fig. S6. Copper ions are not required for the biosynthesis of functional MOR244-3. (*A*) Dose–response curves of MOR244-3 to MTMT with exogenous copper addition at different time points in the luciferase assay. The copper ion effect was lost when copper ion was added at the time of plasmid transfection, and the cells were subsequently subjected to a washing to remove free copper ion before stimulation (green line). (*B*) Copper effect of MOR244-3 is abolished by TEPA despite the timing of addition. Response of MOR244-3 to MTMT with TEPA added either starting at transfection or at stimulation. (*C* and *D*) Copper transporter deficiency does not abolish MOR244-3 copper effect. (*C*) Knockdown efficiency of RNAi of ATP7A and ATP7B compared with intact HEK293T cells. (*D*) Dose–response curves of MOR244-3 to MTMT with or without copper when transfected into ATP7A/B RNAi and intact HEK293T cells. All responses are normalized to MOR244-3's highest response to MTMT.

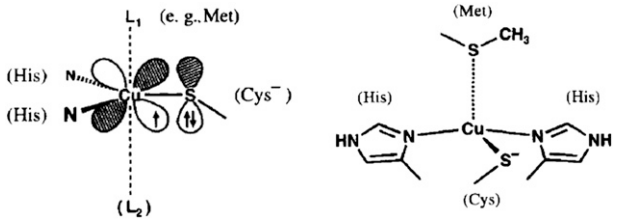

Fig. S7. Bonding in type 1 centers in blue copper proteins azurin (*Left*) and plastocyanin (*Right*) between copper(II) and cysteine thiolate. The drawing for azurin shows the strong-interaction of the thiolate ligand and the electron-deficient metal ion. The coordination is almost optimal for Cu(I), for example, trigonal-planar coordination by cysteinate RS^- with a short Cu–S bond with significant covalent character, two histidine residues, and additional long axial bonds to the weak-acceptor thioether sulfur of methionine (L_1) and a peptide backbone carbonyl group (L_2) (1, 2). This model could equally well represent binding of $X(CH_2)_nSH$ (X = MeS, MeSe, or H_2N; n = 1–3) in the presence of copper ion by MOR244-3, where at least one histidine is required for activity and backbone carbonyl groups are abundant.

1. Block E, Zubieta J (1994) Metal-thiolate coordination chemistry: A bioinorganic perspective. *Advances in Sulfur Chemistry*, ed Block E (JAI Press, Greenwich, CT), pp 131–191.
2. Krebs B, Henkel G (1991) Transition metal thiolates. From molecular fragments of sulfides to models of active centers of biomolecules. *Angew Chem Int Ed* 30:769–788.

Other Supporting Information Files

Table S1 (DOC)
Table S2 (DOC)
Table S3 (DOC)
Table S4 (DOC)
Table S5 (DOC)